JACS
JOURNAL OF THE AMERICAN CHEMICAL SOCIETY
Article
Cite This: J. Am. Chem. Soc. 2019, 141, 19436−19447
pubs.acs.org/JACS

Cooperative Intramolecular Hydrogen Bonding Strongly Enforces *cis*-Peptoid Folding

Andrew W. Wijaya,[†,⊥] Andy I. Nguyen,[*,†,⊥] Leah T. Roe,[†] Glenn L. Butterfoss,[‡] Ryan K. Spencer,[§] Nan K. Li,[†] and Ronald N. Zuckermann[*,†]

[†]The Molecular Foundry, Lawrence Berkeley National Laboratory, 1 Cyclotron Road, Berkeley, California 94720, United States
[‡]Center for Genomics and Systems Biology, New York University Abu Dhabi, Abu Dhabi, United Arab Emirates
[§]Department of Chemistry, Department of Chemical Engineering & Material Science, University of California, Irvine, California 92697, United States

Supporting Information

ABSTRACT: Sequence-defined peptoids, or *N*-substituted glycines, are an attractive class of bioispired polymer due to their biostability and efficient synthesis. However, the *de novo* design of folded peptoids with precise three-dimensional structures has been hindered by limited means to deterministically control backbone conformation. Peptoid folds are generally destabilized by the *cis*/*trans* backbone-amide isomerization, and few side-chains are capable of enforcing a specific amide conformation. Here, we show that a novel class of cationic alkyl ammonium ethyl side-chains demonstrates significant enforcement of the *cis*-amide backbone ($K_{cis/trans}$ up to 70) using an unexpected ensemble of weak intramolecular CH−O and/or NH−O hydrogen bonds between the side-chain and the backbone carbonyl moieties. These interactions are evidenced by X-ray crystallography, variable-temperature NMR spectroscopy, and DFT calculations. Moreover, these side-chains are inexpensive, structurally diverse, hydrophilic, and can be integrated into longer peptoid sequences via solid-phase synthesis. Notably, we extended these concepts to synthesize a water-soluble peptoid 10-mer that adopts one predominant fold in solution, as determined by multidimensional NMR spectroscopy. This decamer, to the best of our knowledge, is the longest linear peptoid sequence atomically characterized to retain a well-folded structure. These findings fill a critical gap in peptoid folding and should propel the development of peptoid applications in a broad range of contexts, from pharmaceutical to material sciences.

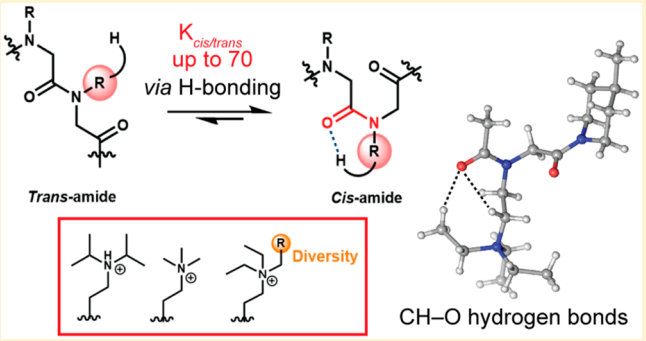

INTRODUCTION

Peptoids, or poly *N*-substituted glycines, are a class of peptidomimetic polymers privileged with uniquely fast, low-cost, and modular synthesis that allows for a wide variety of noncanonical side-chains to be incorporated into an sequence-defined oligomer with high yield and precision.[1−3] As peptoids are resistant to proteolysis,[4] they have been investigated for numerous biological applications such as drug-delivery,[5,6] antifreeze additives,[7] therapeutics,[8] and antimicrobial agents.[9,10] Moreover, amphiphilic peptoid sequences can form novel nanomaterials via supramolecular self-assembly, where the morphology is determined by sequence alone,[11−16] and the surface of these materials can be precisely tuned to display useful functionalities such as pathogen binding.[17,18] However, despite the demand for biomimetic applications with peptoids, the development of new functional peptoids has been hindered by the limited available options to control their folding into well-defined three-dimensional architectures.

A major challenge in controlling peptoid conformation arises from the presence of the tertiary amide bond in the peptoid backbone, which means that each peptoid residue can adopt either of the nearly isoenergetic *cis* or *trans* conformations (rotation about ω) (Figure 1a). This isomerization adds to the flexibility of the peptoid backbone, making it a challenge to create rigid and stable secondary structures. Despite this, several peptoid secondary structures have been reported, all using strategies to control of rotation about ω. These structures include polyproline-type helices with all *cis* (PPI)[19−22] amide bonds, the all *cis* sigma strand,[12] the peptoid ribbon,[23] and the square helix[24] with an alternating amide backbone pattern of *cis* and *trans*. Thus, in order to promote the development of novel peptoid functionalities, we must better understand and extend such strategies to construct new and diverse monomers that promote predictable peptoid folding.

To date, the most reliable way to control the amide isomerization in solution is with specialized side-chains (Figure

Received: September 29, 2019
Published: November 25, 2019

Downloaded via UNIV OF CALIFORNIA SAN FRANCISCO on February 10, 2026 at 18:19:11 (UTC).
See https://pubs.acs.org/sharingguidelines for options on how to legitimately share published articles.

© 2019 American Chemical Society

DOI: 10.1021/jacs.9b10497
J. Am. Chem. Soc. 2019, 141, 19436−19447

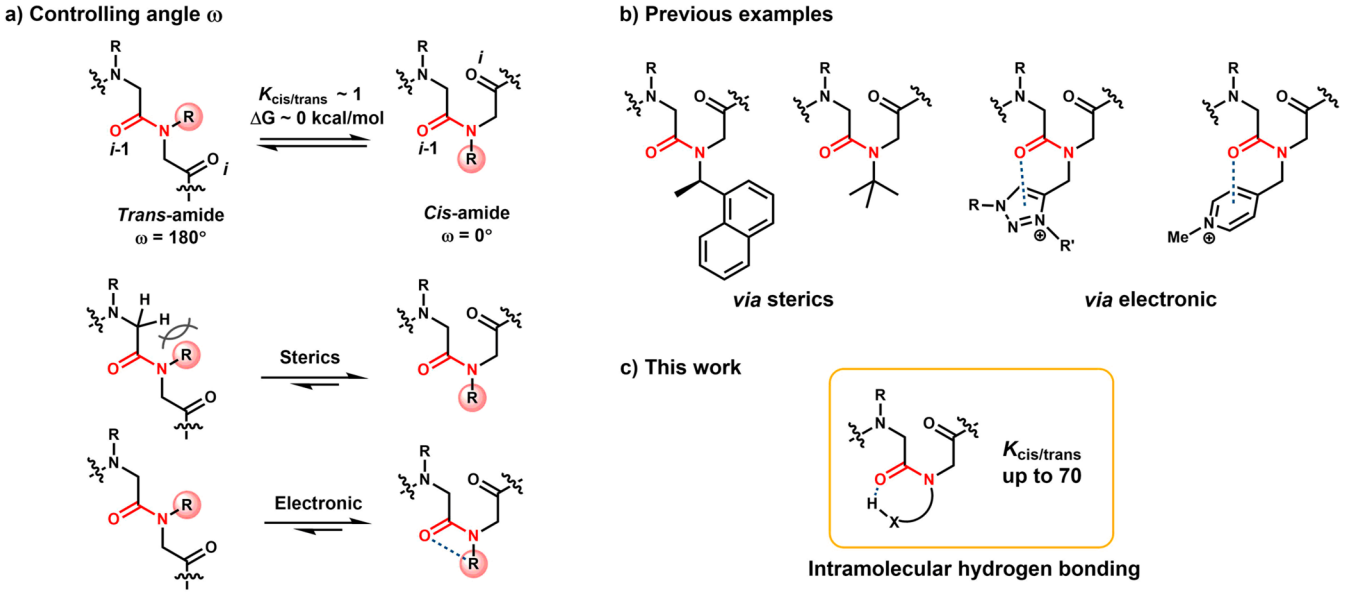

Figure 1. Strategies for backbone *cis*-amide induction. (a) Peptoid backbone dihedral parameter ω controls *trans*- and *cis*-amide conformations. A general approach of tuning ω utilizes sterics and electronic factors by the side-chain. (b) Side-chain examples from the literature include 1-naphthylethyl (1npe),[25] *tert*-butyl (*t*Bu),[26] (benzyltriazolyl)ethyl (bte),[27] and 4-methylpyridinium (4mpy).[25] (c) Our work features engineered side-chains that facilitate intramolecular hydrogen bonds as a means to enforce the backbone *cis*-amide conformation.

1a). A common approach to favor the *cis*-amide conformation is to use extremely bulky, α-branched side-chains that disfavor steric interactions present in the *trans* conformation. A dearth of these side-chains that are also readily available has led to repeated use of the same generally hydrophobic peptoid monomers in generating peptoid structures. For example, the moderately *cis*-inducing ($K_{cis/trans} \approx 6$), chiral 1-naphthylethyl side-chain (N1rnpe or N1snpe) (Figure 1b) is found in nearly all of the peptoid secondary structures mentioned previously.[20,23,24] Additionally, these bulky monomers generally have low monomer addition yields and create overall structures that are too hydrophobic for use in aqueous media. The *tert*-butyl side-chain and its derivatives are also used to control amide bond isomerization through steric interactions, showing preference exclusive to *cis*-amide isomers in all solvents.[26,28] However, these side-chains are extremely nonpolar and are incompatible with solid-phase peptoid synthesis due to the instability of the *tert*-butyl moiety during acid cleavage conditions, precluding their use in longer peptoid sequences.

A separate class of side-chains leverages attractive intramolecular interactions between the amide carbonyl oxygen and the side-chain moiety to stabilize *cis*-amide isomers. This strategy has widely been demonstrated with an n $\rightarrow$ π^* interaction between the side-chain and the carbonyl oxygen of the previous residue ($i-1$ position). The electronic effect originates from the lone pair donation (n orbital) of the $i-1$ carbonyl oxygen to an empty, low-energy antibonding orbital (π^*) of the side-chain (Figure 1b). A recent report demonstrated that fluorination of aromatic residues strengthens this interaction.[29] Potent *cis* induction (up to $K_{cis/trans} \approx 20$) is seen with cationic triazolium and *N*-alkylpyridinium side-chains, as well as side-chains with electrophilic carbonyl moieties.[27,25] Currently, these side-chains are the strongest peptoid *cis* inducers reported in the literature that can be accessed by solid-phase peptoid synthesis. However, a potential drawback of triazolium side-chains are the addition of two extra synthesis steps per monomer incorporation, Cu-catalyzed "click" azide–alkyne cycloaddition (CuAAC) and electrophilic alkylation, which greatly lengthens the time of synthesis. Another strategy leverages inductive effects of fluoroalkyl side-chains to induce moderate *cis*-amide isomers, presumably by dipole–dipole interactions between the side-chain and backbone carbonyl.[30] The ideal structure-inducing peptoid side-chain should therefore be able to strongly enforce a specific backbone conformation, and also be inexpensive, readily available, easily diversifiable, and compatible with a diverse set of side-chains. Furthermore, it should allow for the synthesis of long, water-soluble sequences via the solid-phase submonomer method.

Surprisingly, simple intramolecular hydrogen-bonding between a side-chain and the $i-1$ carbonyl oxygen atom has not been widely recognized in peptoids as a means of stabilizing a specific amide conformation despite the prevalence and importance of hydrogen-bonding in natural biopolymers. Previous studies have experimentally identified instances of CH–O interactions between side-chains and the backbone in peptoids,[26,27,31] but the dominant *cis* induction mechanism was attributed to sterics or n $\rightarrow$ π^* stabilization. The free energy stabilization of a typical hydrogen bond ranges from 1 to 3 kcal/mol,[32,33] and in theory, careful engineering of a hydrogen-bonding interaction between the carbonyl oxygen of the previous residue ($i-1$) to a polarized hydrogen on the side-chain should be able to significantly enforce the *cis*-amide geometry (a factor of 10 increase in $K_{cis/trans}$ per $\Delta G = 1.37$ kcal/mol stabilization).

Herein, we describe a series of cationic side-chains that are both the strongest *cis*-inducing peptoid side-chains reported to date and also amenable to solid-phase synthesis, with $K_{cis/trans}$ up to 70. Notably, all side-chains herein reported are readily available commercially or via simple synthesis (with two steps or fewer from low-cost starting materials), are highly diverse, and also allow for the synthesis of well-folded, water-soluble peptoids. Interestingly, this new class of side-chains interacts with the backbone carbonyl moieties using multiple hydrogen

DOI: 10.1021/jacs.9b10497
J. Am. Chem. Soc. 2019, 141, 19436–19447

Chart 1. Peptoid Monomer Structures[a]

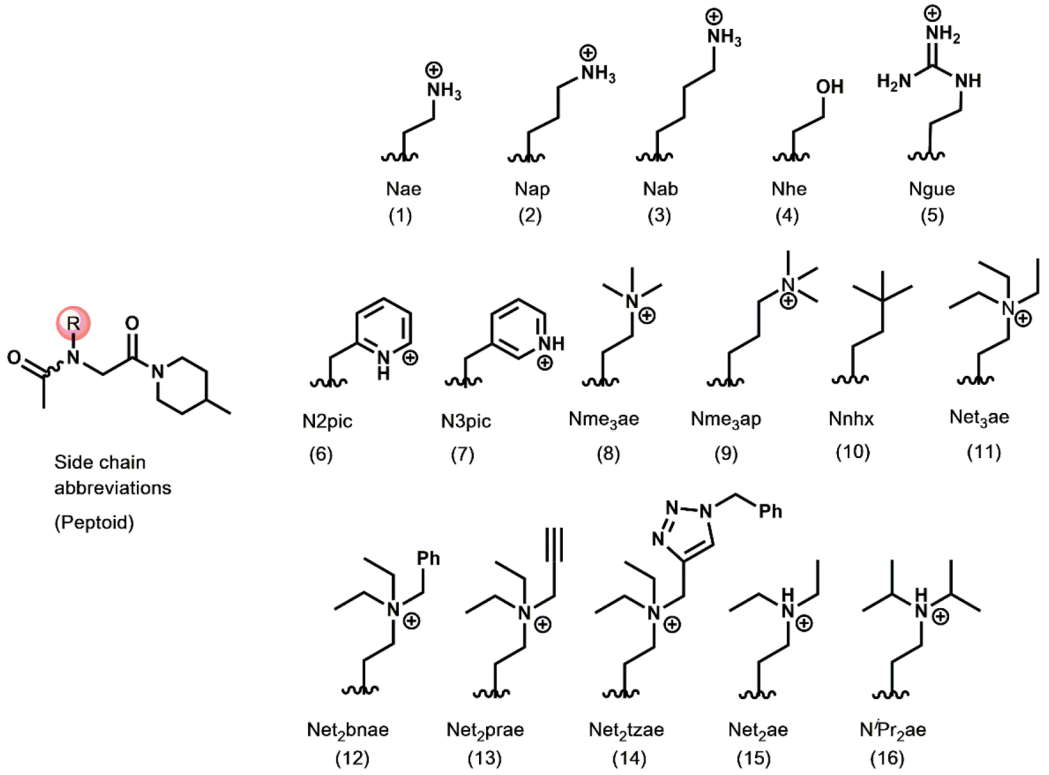

[a]Cationic peptoids are isolated and characterized in their trifluoroacetate (TFA) salt forms.

bonds, which we characterized with variable-temperature NMR spectroscopy, X-ray crystallography, and theoretical calculations. These new monomers allow the synthesis of longer peptoids (up to a 10-mer), which we also structurally characterized with atomic precision by solution NMR spectroscopies. Notably, the peptoid decamer is the longest linear peptoid known to adopt a predominant well-folded secondary structure in solution and showcases peptoid side-chain diversity with 10 individual unique residues. The development of these readily accessible cationic, hydrogen-bonding side-chains is an important milestone for advancing fundamental foldamer chemistry, as well as for the design of structured, water-soluble peptoids for biological and pharmaceutical applications.

RESULTS AND DISCUSSION

Peptoid Monomer Models. Previous studies by Blackwell and Taillefumier utilized a peptoid monomer derivative with an acetyl N-terminus and piperidinyl at the C-terminus to isolate the side-chain interactions with the backbone and used that data to predict the *cis*/*trans* population ($K_{cis/trans}$) in longer peptoid oligomers.[25,27,28] In this study, we utilized a similar system, substituting piperidinyl for 4-methylpiperidinyl, which still allows for direct comparisons with previously reported side-chains. The $K_{cis/trans}$ ratios were determined by integrating ^{1}H NMR resonances of the peptoid, and were measured in a range of solvents ($CDCl_3$, MeOD, and D_2O) to probe the effect of solvent polarity and the presence of proton donors. Peaks for each rotamer were assigned with two-dimensional NMR techniques, including the rotating-frame nuclear Overhauser effect correlation spectroscopy (ROESY) NMR technique to distinguish between the *cis* and *trans* rotamers.

Conventional Hydrogen-Bonding Monomers. We commenced our study by synthesizing and analyzing peptoids that feature a potential NH−O hydrogen-bonding interaction. Previous studies have hinted that side-chains with primary amine or ammonium functionalities tethered to the backbone by an alkyl linker, such as *N*-aminoethyl (Nae), *N*-aminopropyl (Nap), and *N*-aminobutyl (Nab), may be capable of inducing the *cis*-amide geometry in peptoid structures, though these studies did not quantify the extent of *cis* induction.[34,35] Moreover, the mentioned side-chains are widely used in peptoid structures such as in nanosheets and helices.[10,12,36] Peptoid monomer derivatives, **1**−**3**, containing Nae, Nap, and Nab, respectively, were synthesized to test this hypothesis, along with other peptoids as controls, *N*-hydroxyethyl (Nhe) (**4**), *N*-guanidinylethyl (Ngue) (**5**), *N*-2picolyl (N2pic) (**6**), and *N*-3picolyl (N3pic) (**7**) (Chart 1). Indeed, most of these side-chains favor the *cis*-amide geometry moderately ($K_{cis/trans}$ up to 5.4), with the exception of Nhe (**4**), which slightly favors the *trans* rotamer ($K_{cis/trans}$ = 0.9 in $CDCl_3$, 0.5 in MeOD and D_2O), and Nab (**3**), which shows almost no preference for either geometry in all solvents ($K_{cis/trans} \approx 1$) (Table 1).

Comparing the side-chains with N−H moieties, the trend of monomers that show *cis* induction follows **2** > **1** > **5** > **3**. The intramolecular hydrogen bond ring size with the backbone carbonyls leads to a hydrogen bond donor competition between the $i - 1$ and i carbonyls, whereby only the interaction with the $i - 1$ carbonyl should affect the *cis*/*trans* ratio (Figure 2a). Density-functional theory (DFT) models of **1**−**3** and **5** reproduce the experimentally observed ordering of *cis* favorability (the monomers used for *in silico* work have an *N*,*N*-dimethyl rather than a 4-methylpiperidinyl C-terminus) and showcase the expected intramolecular hydrogen-bonding

DOI: 10.1021/jacs.9b10497
J. Am. Chem. Soc. 2019, 141, 19436−19447

Table 1. $K_{cis/trans}$ Values of Peptoid Monomers[a]

monomers		$CDCl_3$		MeOD		D_2O	
no.	R group	$K_{cis/trans}$	ΔG	$K_{cis/trans}$	ΔG	$K_{cis/trans}$	ΔG
1	Nae	1.9	−0.38	2.4	−0.52	2.2	−0.47
1[b]	Nae neutral	1.0	0.00	2.2	−0.47	1.9	−0.38
2	Nap	3.1	−0.67	3.0	−0.65	2.1	−0.44
2[b]	Nap neutral	1.0	0.00	1.5	−0.24	1.0	0.00
3	Nab	1.0	0.00	1.0	0.00	0.9	0.06
3[b]	Nab neutral	0.8	0.13	1.3	−0.16	1.0	0.00
4	Nhe	0.9	0.06	0.5	0.41	0.5	0.41
5	Ngue	2.0	−0.41	1.5	−0.24	1.2	−0.11
6	N2pic	5.4	−1.00	4.2	−0.85	3.2	−0.69
6[b]	N2pic neutral	0.5	0.41	1.1	−0.06	1.0	0.00
7	N3pic	4.3	−0.86	3.7	−0.77	2.2	−0.47
7[b]	N3pic neutral	0.6	0.30	1.6	−0.28	1.3	−0.16
8	Nme_3ae	22	−1.83	6.1	−1.07	4.1	−0.84
9	Nme_3ap	4.7	−0.92	2.1	−0.44	1.7	−0.31
10	Nnhx	0.2	0.95	0.5	0.41	–[c]	–[c]
11	Net_3ae	70	−2.52	14	−1.56	5.8	−1.04
12	Net_2bnae	70	−2.52	15	−1.60	6.1	−1.07
13	Net_2pgae	40	−2.32	8.8	−1.29	4.4	−0.88
14	Net_2tzae	60	−2.42	8.5	−1.27	4.9	−0.94
15	Net_2ae	13	−1.52	9.4	−1.33	5.4	−1.00
15[b]	Net_2ae neutral	0.3	0.71	0.8	0.13	0.8	0.13
16	N^iPr_2ae	30	−2.01	16	−1.64	8.1	−1.24
16[b]	N^iPr_2ae neutral	0.3	0.71	0.7	0.21	0.8	0.13

[a] $K_{cis/trans}$ values in different solvents ($CDCl_3$, MeOD, and D_2O) and their corresponding free energy differences (ΔG in kcal/mol) of peptoid monomers **1**−**16**. $K_{cis/trans}$ values are generally calculated using two sets of ^1H NMR resonances. $K_{cis/trans}$ values ≥ 40 are rounded to the nearest ten. [b] Deprotonated to its neutral state. [c] Insoluble in solvent.

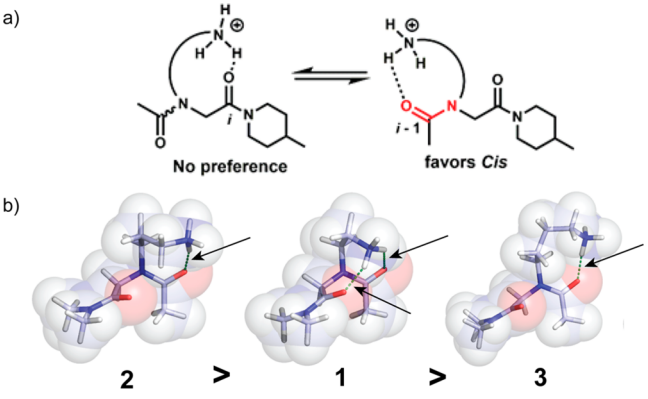

Figure 2. Hydrogen-bonding hypothesis. (a) Hydrogen bond competition between the backbone carbonyls where interactions with $i-1$ carbonyl O will favor the *cis*-amide conformation. (b) Energy-minimized structures of **1**−**3** (derived at the B3LYP/6-311++G(2d,2p)[37] level of theory in implicit water) showcase NH−O bond interactions (dotted green line, marked with black arrow) between the side-chains and the backbone carbonyls with differing ring size.

interactions (Figure 2b). The predicted relative potential energies for the best-identified *cis* versus best-identified *trans* conformations give the *cis* preference rank order as **2** (−1.55 kcal/mol) > **1** (−1.00 kcal/mol) > **5** (−0.44 kcal/mol) > **3** (0.02 kcal/mol). Moreover, as expected with hydrogen-

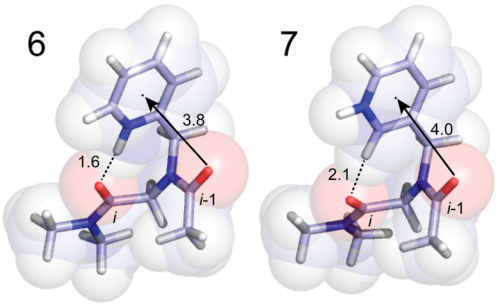

Figure 3. Energy-minimized structures of peptoid **6** and **7**. Lowest energy conformations (**6** pictured left, **7** pictured right) derived at the B3LYP/6-311++G(2d,2p) level of theory[37] in implicit water feature an intramolecular hydrogen bond (dotted line with $i-1$ carbonyl) and an n → π^* interaction (arrow with i carbonyl) facilitated by the pyridyl side-chain; the interaction distances are shown in angstroms.

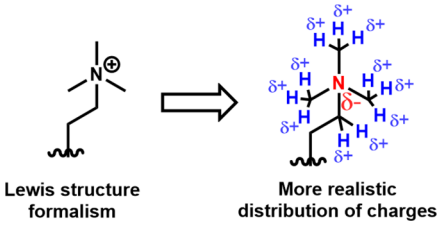

Figure 4. Comparison between Lewis structure and a more realistic charge distribution in an Nme_3ae side-chain. Formal Lewis structure fails to depict the distribution of Mulliken charges in the Nme_3ae side-chain. The α-protons of the ammonium core are positively charged (blue), while the negative charge (red) is concentrated on the nitrogen.

bonding, deprotonation of the amines in peptoids **1** and **2** by addition of 1 equiv of KOH also reduces the *cis*-population from 66% and 75%, respectively, to 50% for both **1**[b] and **2**[b] (in $CDCl_3$).

The difference of $K_{cis/trans}$ values between Nae (**1**) and Ngue (**5**) also suggests that the geometry of the N−H proton is a relevant factor for *cis* induction. Compound **1** has an sp^3-hybridized nitrogen with a tetrahedral geometry, whereas the nitrogen of **5** is sp^2 hybridized with a trigonal planar geometry. Our models suggest that the planarity significantly increases the ring strain of the seven-membered ring formed between the guanidine N−H and the $i-1$ carbonyl, preventing a proper hydrogen bond to take place (see Supporting Information). In the DFT models, the guanidinium side-chain of **5** makes a hydrogen bond to the i carbonyl in both the most favorable *cis* and *trans* conformations (which are nearly isoenergetic). A *cis* conformation with a hydrogen bond to the $i-1$ carbonyl is 1.2 kcal/mol higher in energy, supporting the prediction that the Ngue side-chain of **5** is too restricted to promote *cis*.

The *N*-picolyl monomers, **6** and **7**, also show moderate *cis* induction ($K_{cis/trans}$ up to 5.4 and 4.3 for **6** and **7**, respectively). However, unlike the amino alkyl side-chains, these side-chains are capable of also forming an n → π^* interaction with the $i-1$ backbone carbonyl, similar to the (benzyltriazolyl)ethyl (bte) and 4-methylpyridinium (4mpy) side-chains.[25,27] Therefore, *cis* induction to some degree should be present for both **6** and **7**, and the observed $K_{cis/trans}$ values cannot be attributed to solely hydrogen bonding. DFT models based on **6** and **7** predict that both side-chains prefer similar rotameric states. The ring forms either a pyridyl NH−O hydrogen bond (in **6**) or an aromatic

DOI: 10.1021/jacs.9b10497
J. Am. Chem. Soc. 2019, 141, 19436−19447

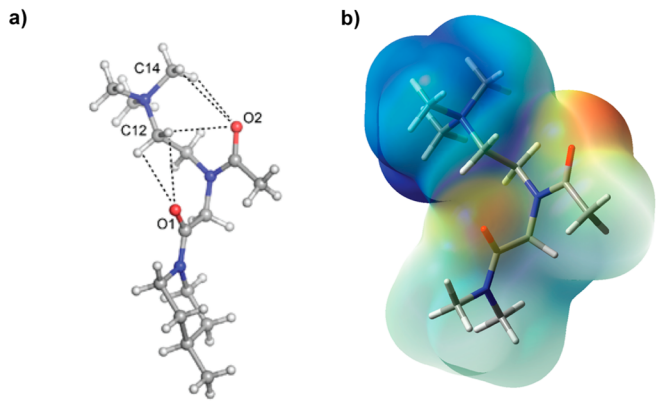

c)

Interaction	Distance C–O (Å)	Angle (°)
C14–H···O2	3.344 (2)	101 (2), 106 (2)
C12–H···O2	3.042 (2)	110 (2)
C12–H···O1	3.3791 (1)	97 (2), 102 (2)

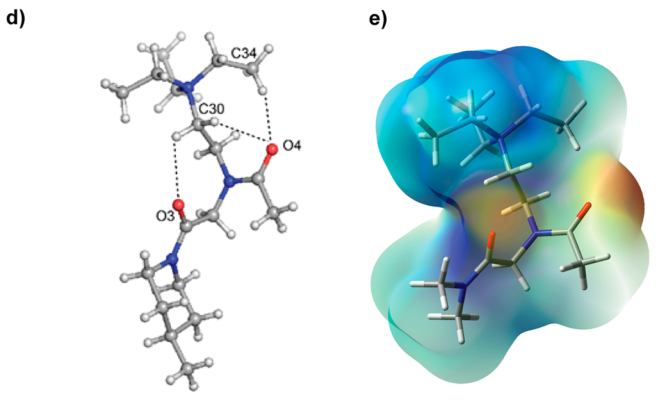

f)

Interaction	Distance C–O (Å)	Angle (°)
C34–H···O4	3.483 (3)	164 (3)
C30–H···O4	3.005 (3)	116 (3)
C30–H···O3	3.340 (3)	121 (3)

Figure 5. Crystallographic and DFT structures of peptoids **8** and **11**. (a) Solid-state structure of peptoid **8** in ball-and-stick representation. Only one isomer out of two in the asymmetric unit is shown here; BPh_4 anion and toluene molecules are omitted for clarity. Hydrogen bonds are drawn as dotted lines. (b) Electrostatic potential surface (EPS) map of the most favorable DFT structure of peptoid **8**. Color scheme: blue indicates higher positive potential; color intensity is proportional to the magnitude of the charge. (c) Parameters of hydrogen-bonding interactions in peptoid **8** as observed in the solid state. Distance cutoff for CH−O interactions is 3.7 Å between the donor and acceptor atom. (d) Solid-state structure of peptoid **11** in ball-and-stick representation. Only one isomer out of four in the asymmetric unit is shown here; BPh_4 anions are omitted for clarity. Hydrogen bonds are drawn as dotted lines. (e) Electrostatic potential surface (EPS) map of the most favorable DFT structure of peptoid **11**. Color scheme: blue indicates more positively charged; color intensity is proportional to the magnitude of the charge. (f) Parameters of hydrogen-bonding interactions in peptoid **11** as observed in the solid state. Distance cutoff for CH−O interactions is 3.7 Å between the donor and acceptor atom.

CH−O hydrogen interaction (**7**) with the *i* carbonyl. The *cis* state of both appears to be promoted via n → π^* interaction interactions between the $i-1$ carbonyl and the pyridyl ring rather than a hydrogen bond; however, the intramolecular hydrogen bond interaction with the *i* carbonyl may assist in *cis* induction by forcing the ring to be perpendicular with respect to the $i-1$ carbonyl, thus maximizing the n → π^* donation (Figure 3). A similar motif to induce *cis* has been previously observed in the N(benzyltriazolyl)ethyl (Nbte) monomer.[27]

The existence of attractive electrostatic interactions to induce *cis* in **1**, **2**, **6**, and **7** is further supported by the decrease of $K_{cis/trans}$ values of these monomers in more polar solvents ($K_{cis/trans}$ up to 5.4 in CD_3Cl versus $K_{cis/trans}$ up to 3.2 in D_2O). For cases with hydrogen bonding, polar protic solvents are able to participate in hydrogen-bonding donation and acceptance, which competes with the intramolecular peptoid hydrogen bond. Overall, moderate *cis* induction has been observed with four side-chains in the monomeric system: *N*-aminoethyl (Nae), *N*-aminopropyl (Nap), *N*-2-picolyl (N2pic), and *N*-3-picolyl (N3pic). The existence of *cis*-inducing electrostatic interactions in these monomers is consistent with the observed trend in ring size, amine proton geometry, protonation state, and solvent polarity.

Quaternary Ammonium Side-Chains. To further test our hypothesis that hydrogen bonding with the backbone promotes *cis*-amides, we removed all of the N−H moieties of **1** and **2** via exhaustive alkylation, forming quaternary ammonium functionalities. We postulated that the absence of N−H protons should decrease the $K_{cis/trans}$ values as the side-chains can no longer facilitate classical hydrogen bonds to the backbone carbonyls. Alkylation of peptoids **1** and **2** with excess iodomethane yielded peptoids **8** and **9** with side-chains *N*-trimethylammonium-ethyl (Nme_3ae) and *N*-trimethylammonium-propyl (Nme_3ap), respectively.

Surprisingly, peptoid **8** has an extraordinarily high $K_{cis/trans}$ of 22 in $CDCl_3$, about 10 times higher than that of **1**. In polar protic solvents, the *cis* isomer of **8** remained heavily predominant ($K_{cis/trans}$ = 6.1 in MeOD and 4.1 in D_2O), which is higher than the popular 1-naphthylethyl side-chain ($K_{cis/trans}$ = 4.6 in MeOD). Similarly, the $K_{cis/trans}$ values of **9** are also increased with respect to **2** ($K_{cis/trans}$ = 4.7 in $CDCl_3$), albeit much more modestly. This strength of induction between **8** and **9** indicates that the alkyl tether length is a principal factor for *cis* induction in this system, similar to the peptoids that contained N−H donors.

To control for potential steric effects of the larger Nme_3ae side-chain (relative to Nae), we synthesized an isosteric derivative of **7**, peptoid **10**, which contains a neutral *N*-neohexyl side-chain (Nnhx). The $K_{cis/trans}$ values of **10** are significantly less than 1 in all solvents ($K_{cis/trans}$ = 0.2 and 0.5 in CD_3Cl and MeOD, respectively), indicating that the *trans* isomer is favored for this isosteric compound. This observation dictates that the *cis*-directing effect of the Nme_3ae side-chain is not due to sterics, but rather an electronic effect induced by the quaternary ammonium moiety. In this regard, it is especially important to recognize a more realistic distribution of charges in quaternary ammonium moieties. The positive charge of a quaternary ammonium moiety is known to be delocalized among the protons surrounding the ammonium core and not on the nitrogen, as traditionally depicted in formal Lewis structures (Figure 4).[38]

Motivated by the potent *cis* induction of the Nme_3ae side-chain, we prepared several other peptoids containing novel quaternary ammonium side-chains, each tethered to the backbone by an ethylene linker: *N*-triethylammonium-ethyl

DOI: 10.1021/jacs.9b10497
J. Am. Chem. Soc. 2019, 141, 19436−19447

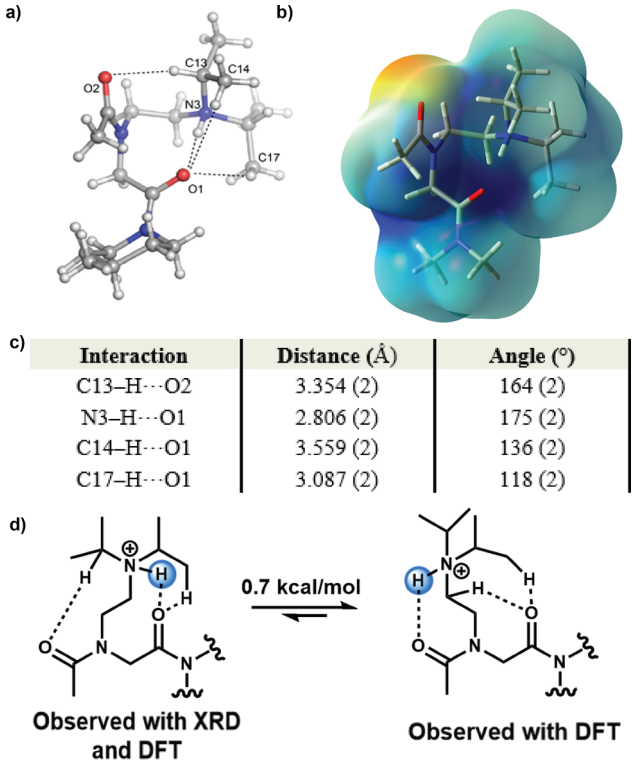

Figure 6. Crystallographic and DFT structures of peptoid **16**. (a) Solid-state structure of peptoid **16** in ball-and-stick representation. BPh_4 and toluene molecules are omitted for clarity. Hydrogen bonds are drawn as dotted lines. (b) Electrostatic potential surface (EPS) map of the most favorable DFT structure of peptoid **16**. (c) Parameters of hydrogen-bonding interactions in peptoid **16** as observed in the solid state. Distance cutoff for CH−O interactions is 3.7 Å between the donor and acceptor atom. (d) Potential equilibrium process between two intramolecular hydrogen-bonding motifs facilitated by a N^iPr_2ae side-chain. The amine hydrogen atom is highlighted with a blue circle and interacts favorably with both the *i* carbonyl (left) and the *i* − 1 carbonyl (right). Barrier of isomerization is small (0.7 kcal/mol), as estimated by DFT computations.

Table 2. Thermodynamic Parameters of *Cis* Induction in Peptoids 8, 11, 12, and 16

peptoid	ΔH (kcal/mol)	$-T\Delta S$ (kcal/mol)[a]
8	+0.50(6)	−1.33(6)
11	−0.66(3)	−0.67(3)
12	−0.71(3)	−0.70(3)
16	−0.52(3)	−0.62(3)

[a] $-T\Delta S$ is calculated at 298 K.

(Net_3ae) (**11**), *N*-diethylbenzylammonium-ethyl (Net_2bnae) (**12**), *N*-diethyl-propargylammonium-ethyl (Net_2pgae) (**13**), and *N*-diethyl-triazoleammonium-ethyl (Net_2tzae) (**14**). Overall, these derivatives demonstrate exceptionally high $K_{cis/trans}$ values ($K_{cis/trans}$ = 40−70 in CD_3Cl, $K_{cis/trans}$ = 8.5−15 in MeOD, and $K_{cis/trans}$ = 4.4−6.1 in D_2O).

The *cis* induction of peptoids **11** and **12** is consistently stronger ($K_{cis/trans} \approx 15$ in MeOD and $K_{cis/trans} \approx 6$ in D_2O) than the best reported in the literature, chiral triazolium-type side-chains, even in polar protic solvents ($K_{cis/trans}$ = 11.1 in MeOD and 5.5 in D_2O for Nbte).[27] Notably, **14** was derived from **13** via CuAAC "click" reaction.[39] Click chemistry can greatly increase diversity of the side-chain via azide-partner

Scheme 1. Optimized Amine Precursor Synthesis for Net_3ae, Net_2bnae, and Net_2pgae Side-Chains

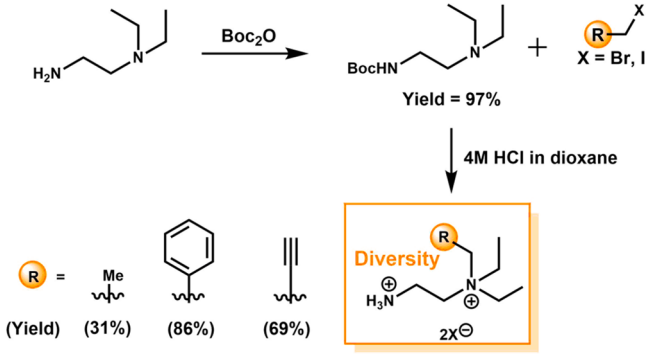

Scheme 2. Optimized Solid-Phase Peptoid Synthesis with Quaternary Ammonium Side-Chains[a]

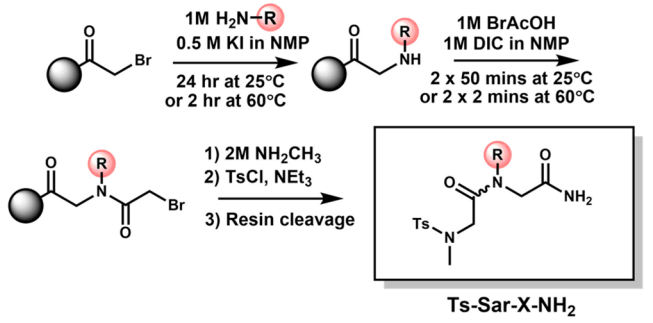

[a] Optimized quaternary ammonium-type side-chains (R) include Nme_3ae (**17**), Net_3ae (**18**), Net_2bnae (**19**), and Net_2pgae (**20**). Full synthetic details are catalogued in the Supporting Information.

Scheme 3. Ketopiperazinium Formation with Net_2ae

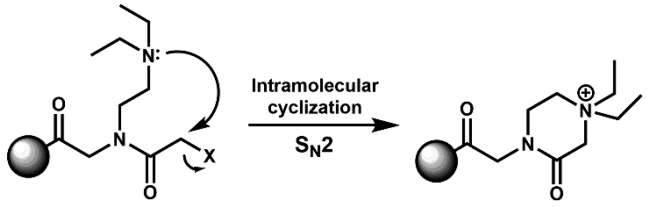

selection alone, providing diverse functionalities for a broad range of potential applications. Overall, the high $K_{cis/trans}$ values demonstrated by peptoids **8** and **11**−**14** indicate that the quaternary ammonium cores facilitate a major electronic effect to enforce the *cis*-amide backbone geometry.

Evidence for a *cis*-stabilizing electronic effect was observed in the solid-state structure. X-ray diffraction on single crystals of tetraphenylborate (BPh_4^-) salts of **8** and **11** show that the peptoids crystallize in their *cis* rotamer state. The backbone dihedral parameters of **8**·BPh_4 fall into the low-energy regions of the *cis* peptoid Ramachandran plot: ψ = 180.8 (1)°, φ = 76.6 (1)°, ω = 6.0 (1)° (Z_{Rc} region).[40] Note that typical peptoid Ramachandran dihedral angles are ψ (180°), φ (90°), and ω (0° for *cis* and 180° for *trans*).[41] The side-chain ethylene linker has an *anti*-conformation, positioning the quaternary ammonium group of Nme_3ae onto the backbone carbonyls. Similarly, **11**·BPh_4 also shows backbone dihedral angles that are typical of peptoids (ψ (187.5(3)°), φ (84.9(2)°), and ω (0.8(3)°)) and also features an *anti*-ethylene side-chain for Net_3ae.

DOI: 10.1021/jacs.9b10497
J. Am. Chem. Soc. 2019, 141, 19436−19447

Chart 2. Ribbon Peptoid Chemical Structures[a]

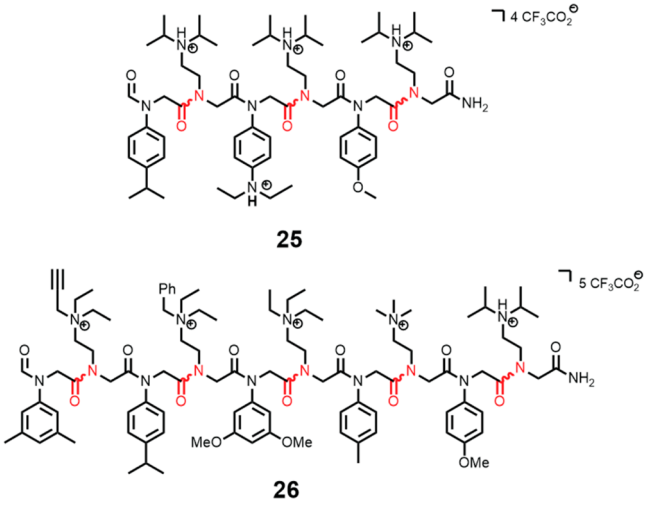

[a]Red amide bonds indicate *cis*-geometry at that position.

Table 3. Folded Populations of Designed Ribbon Peptoids[a]

peptoid	population in MeOD (%)	population in D_2O (%)
25	63	50
26	52	59

[a]Population ratios were calculated by peak fitting the formyl NMR signals.

The solid-state structures also show several short intra- and intermolecular CH−O contacts from the both the *i* and *i* − 1 carbonyl O atoms to the either *α* or *β* protons of the quaternary ammonium moieties (*α* and *β* denote positions relative to the ammonium N atom). Similar CH−O hydrogen bonds have already been reported and observed in numerous crystal structures of synthetic and biological systems.[42−49] For **8·BPh$_4$**, the *i* − 1 (acetyl) carbonyl O has three intramolecular CH−O contacts with the Nme$_3$ae side-chain that are significantly shorter than the sum of their atomic van der Waals radii (3.7 Å). This observation is consistent with CH−O hydrogen bonding between the positively polarized hydrogen atoms *α* to N and the *i* − 1 carbonyl O, stabilizing the *cis*-amide isomer.[50,51] Two additional CH−O contacts between the quaternary ammonium group of Nme$_3$ae with its *i* carbonyl are also observed. These interactions likely act cooperatively to induce the *cis* isomer by positioning the side-chain to favorably interact with the *i* − 1 carbonyl.

The crystal structure conformation of **8** is also favored in DFT calculations. The two most favorable structures identified in a monomer model of **8** correspond to the torsional states observed in the crystal structure, supporting the role of *cis* stabilization via polar CH−O interactions. The polarization can be visualized in the electrostatic potential surface (EPS) of the molecule (Figure 5b), which is positive over the entirety of the side-chain electron isodensity surface. The structure-inducing role of polarization is also supported by the fact that a model of **10**, the neutral isosteric variant of **8**, is predicted to be isoenergic between the *cis* and *trans* states (see Supporting Information), also in line with experimental results.

Similar observations are also seen in the X-ray crystal structure of **11·BPh$_4$** with CH−O interactions from the *β* protons of the ethyl groups, instead of the *α* protons, with the acetyl carbonyl. The *β* protons extend further away from the ammonium core than the *α* protons, allowing them to interact with the acetyl carbonyl at a better geometry (D(C−O) = 3.483 (3) Å, θ(C−H$_\beta$···O) = 164(3)° in **11·BPh$_4$** compared to D(C−O) = 3.344(2) Å, θ(C−H$_\alpha$···O) = 101(2)° and 106(2)° in **8·BPh$_4$**). Note that for hydrogen bonds, the optimal X−H−O angle is linear (180°), and deviation from this angle generally decreases the strength of hydrogen-bonding interactions.[52] These interactions can also be observed in the DFT-computed structures, where the EPS map highlights the positive nature of the *α* and *β* protons on the ethyl groups, supporting the role of electrostatic stabilization of the *cis* state (Figure 5e). Additionally, DFT models of **12** (Net$_2$bnae side-chain) suggest that while the benzyl group may be sterically hindered from interacting directly with the *i* − 1 amide, the observed increases on *cis/trans* preferences relative to **11** are likely due to polarization changes introduced by the ring (see Supporting Information).

Overall, these data suggest that, while an individual CH−O is weak, the quaternary ammonium group allows for an ensemble of polarized C−H moieties to interact simultaneously with the carbonyl O atoms, which may explain the remarkably strong *cis* induction of these side-chains over their primary ammonium counterparts.

Tertiary Ammonium Side-Chains. A potential drawback of quaternary ammonium side-chains is that because an individual CH−O bond is approximately half as strong as an NH−O bond, the efficiency of *cis* induction can be significantly reduced in aqueous solution.[53,54] Maintaining a high degree of *cis* induction in aqueous media remains crucial for foldamer applications, as the majority of biological applications require aqueous and buffered media. We envisioned that a synergy between two types of hydrogen bonds, CH−O and NH−O, could create side-chains that persist better in the presence of polar protic solvent. Tertiary amine moieties, which are generally protonated at pH 7, were hypothesized to facilitate both an NH−O bond with its amine proton and CH−O bond with its polarized *α* or *β* protons.

We first synthesized peptoid **15**, containing a protonated *N*-diethylamino-ethyl (Net$_2$ae) side-chain, as a precursor toward **12** and **13**. We noticed that **15**'s *cis* induction was somewhat strong ($K_{cis/trans}$ up to 13). Motivated by this observation, we synthesized a bulkier derivative, **16**, which features the protonated *N*-diisopropylamino-ethyl (N^{i}Pr$_2$ae) side-chain. We postulated that the polarized C−H, as well as the N−H groups, will be more protected from solvation and will be able to interact more strongly with the backbone carbonyls. Consistent with our hypothesis, the $K_{cis/trans}$ values of **16** ($K_{cis/trans}$ = 30 in $CDCl_3$) were increased approximately 3-fold with respect to **15**. Although the *cis* induction of **16** in nonpolar media such as $CDCl_3$ is not as potent as the quaternary-ammonium side-chains ($K_{cis/trans} \approx 20-70$), this side-chain shows exceptionally large $K_{cis/trans}$ values in polar protic solvents ($K_{cis/trans}$ = 16.0 and 8.1 in MeOD and D_2O, respectively). To date, these values are the highest $K_{cis/trans}$ values of all reported peptoid side-chains achieved in MeOD and D_2O. Furthermore, the important role of the N−H amine proton at enforcing the *cis*-amide geometry was evidenced by very low $K_{cis/trans}$ values of the deprotonated, neutral version of **16** (0.3, 0.7, and 0.8 in $CDCl_3$, MeOD, and D_2O, respectively).

The solid-state structure of **16·BPh$_4$**, as determined by X-ray crystallography, gives evidence of synergistic NH−O and CH−O interactions between the side-chain and backbone (Figure 6). To our surprise, the stronger NH−O bond is formed with

DOI: 10.1021/jacs.9b10497
J. Am. Chem. Soc. 2019, 141, 19436−19447

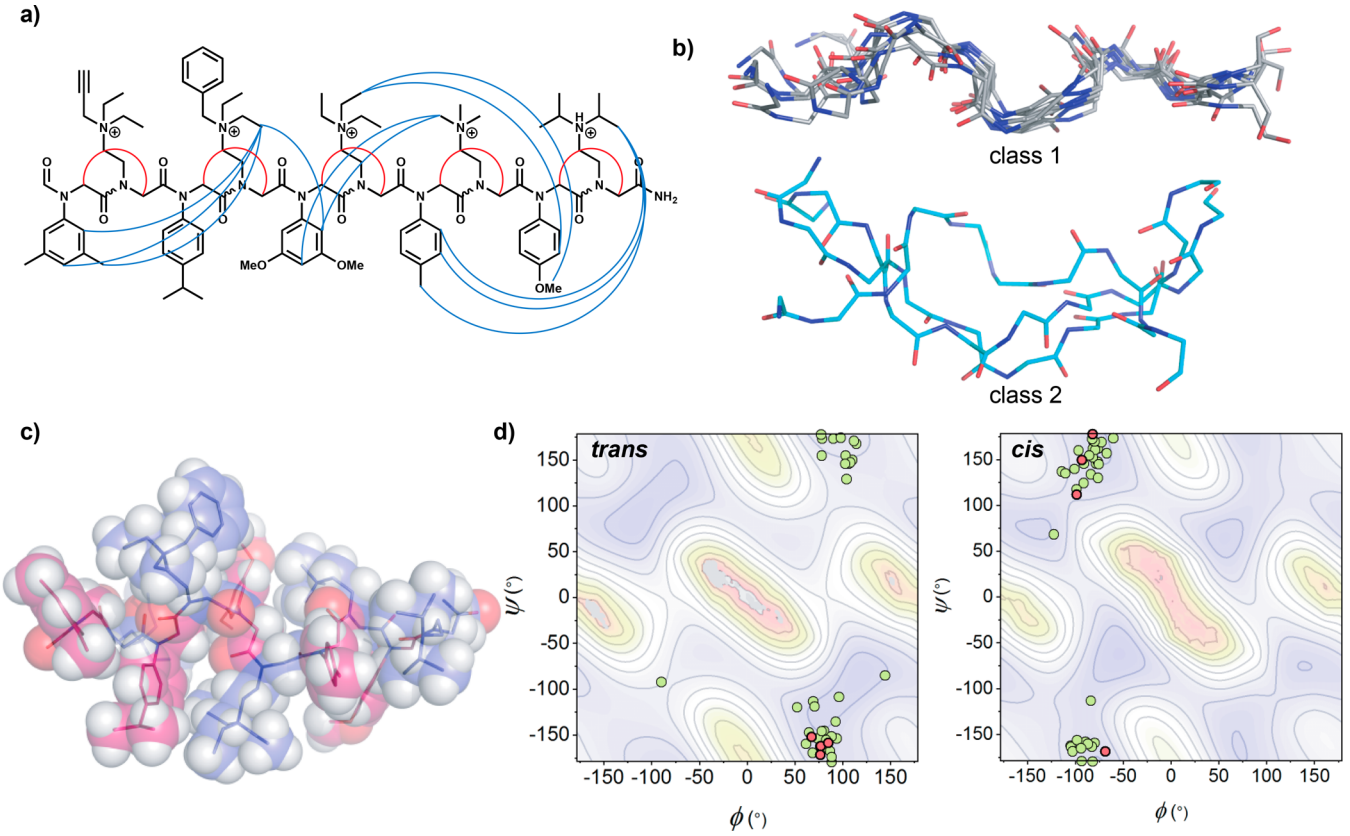

Figure 7. Structural analyses of peptoid **26** in solution. (a) Inter-residue NOE constraints used for REMD structural solution. Blue lines are side-chain-to-side-chain correlations, and red lines are backbone-to-backbone correlations. (b) Ensemble of the 10 lowest energy structures; backbone shown only for clarity. Class 1 structures form the ribbon secondary structure. Class 2 have less regular structure. (c) Space-filling representation of the lowest energy structure. Magenta residues have *N*-aryl side-chains, and blue residues have quaternary ammonium side-chains. (d) *Cis* and *trans* Ramachandran plots of the 10 lowest energy structures from residues 1−9. Green points are dihedral combinations of all structures, and red points are those from the lowest energy structure.

the *i* carbonyl rather than the *i* −1 carbonyl, leaving the polarized methine C−H to interact with the remaining acetyl carbonyl. Moreover, two protons of the ammonium core (on C14 and C17) are also within close proximity to the *i* carbonyl, suggesting that four hydrogen bonds are working cooperatively to favor the *cis*-acetamide conformation. Cooperative interactions also resulted in the side-chain ethylene linker to adopt a *gauche* conformation, rather than an *anti* conformation as seen in previous structures of **8**·BPh_4 and **11**·BPh_4. The backbone dihedral parameters also fall within the typical range for peptoids: ψ = 156.3(1)°, φ = −74.2(2)°, ω = 10.1(2)° (Z_{Sc}).[40]

Likewise, DFT computations on peptoid **16** reveal the conformation observed in the crystal structure is among the three lowest energy structures identified (all three of which are *cis*). Surprisingly, the side-chains in the other two low-energy conformations hydrogen bond with the *i* − 1 (rather than the *i*) carbonyl oxygen (Figure 6). This suggests that the $NiPr_2$ae side-chain is flexible at room temperature, being able to switch between different hydrogen-bonding modes, all of which favor the *cis*-amide isomer at the *i* − 1 position. This appears to be possible because the side-chain can simultaneously form NH−O and CH−O hydrogen bond interactions with both surrounding carbonyl oxygens simultaneously.

Thermodynamic Data. The changes in $K_{cis/trans}$ values with varying temperature experiments allowed extraction of the enthalpic (ΔH) and entropic (ΔS) contributions to folding (Table 2). Van't Hoff plots of these peptoids were constructed from $K_{cis/trans}$ values taken in DMSO from 296 K to 353−373 K (see Supporting Information).

The *cis* induction by Nme_3ae in peptoid **8** is actually slightly endothermic, but the large entropy factor makes the folding spontaneous (ΔH = +0.50 (±0.06) kcal/mol, $-T\Delta S$ = −1.33 (±0.06) kcal/mol at 298 K). The positive ΔH value dictates that interactions in peptoid **8** are enthalpically disfavored, meaning intramolecular interactions are weaker than intermolecular interactions with solvent.[55,56] However, multiple simultaneous intramolecular interactions are able to release more solvent molecules, which accounts for the significant entropy gain, a phenomenon analogous to the hydrophobic effect[57] and metal chelation.[58,59] Although an individual CH−O bond is relatively weak, an ensemble of such interactions between the side-chain and backbone are able to release solvent molecules that were previously interacting with the quaternary ammonium core and carbonyl O.

In contrast to peptoid **8**, peptoid **11** and **12**'s *cis* inductions are exothermic (ΔH = −0.66 (±0.03) kcal/mol and −0.71 (±0.03) kcal/mol, respectively). However, peptoids **11** and **12** still demonstrate entropic gain as a significant factor in their *cis* induction ($-T\Delta S$ = −0.67 (±0.03) kcal/mol and −0.70 (±0.03) kcal/mol at 298 K, respectively). Here, the interaction between the $-CH_3$ moiety of the ethyl group with the carbonyl is stronger than in Nme_3ae, due to a more favorable geometry (*vide supra*), resulting in a slightly exothermic interaction.

DOI: 10.1021/jacs.9b10497
J. Am. Chem. Soc. 2019, 141, 19436−19447

However, the entropy gain is smaller than that of **7**, possibly because **11** and **12** must freeze the rotation of an ethyl group on the side-chain in order to interact with the acetyl carbonyl.

Similar to peptoids **11** and **12**, peptoid **16**'s *cis* induction is also both exothermic and entropy-driven (ΔH = −0.52 (±0.03) kcal/mol, $-T\Delta S$ = −0.62 (±0.03) kcal/mol at 298 K). The presence of a classical NH−O interaction, as seen in the crystal structure, might account for the exothermic *cis* induction. Again, entropy is the major driving force for this process. Altogether, entropic considerations are consistent with the multiple, intramolecular contacts observed in the crystal structures of **8·BPh$_4$**, **11·BPh$_4$**, and **16·BPh$_4$** and DFT results on **8**, **11**, **12**, and **16**.

Synthesis of Longer Peptoid Sequences. *Amine Precursor Synthesis.* To prepare longer sequences by the submonomer method, the side-chains are prepared in their primary amine forms to accommodate the S_N2 displacement step.[1] For some of these side-chains—Nme$_3$ae, Net$_2$ae, and N^{i}Pr$_2$ae—the primary amine submonomers are commercially available and can be purchased at reasonable costs. The other monomers can be easily prepared in gram scale via simple synthesis (with two steps or fewer from low-cost starting materials) as demonstrated herein (Scheme 1).

Solid-Phase Peptoid Synthesis Optimization. We then optimized the conditions for solid-phase synthesis of peptoids comprising our new monomers by testing the synthesis of 2-mer sequences with the general structure Ts-Sar-X-NH$_2$ (Ts = *p*-toluenesulfonyl, Sar = *N*-methylglycine) (Scheme 2).[1] Our initial attempt at incorporating the quaternary ammonium-type monomers into the peptoid sequence on Rink-amide MBHA polystyrene resin using standard conditions (25 °C, acylation with 1.0 M bromoacetic acid/DIC for 10 min, and displacement with 1.0 M amine for 60 min) was low yielding (<30% by HPLC), presumably due to the very low basicity and nucleophilicity of the primary amines (e.g., pK_a of cholamine is 7.1).[60] This problem was mitigated by the introduction of 0.5 M KI to the amine solution (to generate *in situ* a more reactive iodoacetyl electrophile) and extending the displacement step to 24 h at 25 °C. The bromoacylation onto the quaternary ammonium-containing monomer was also double coupled (50 min each), again due to the poor basicity of the N-terminus. Alternatively, synthesis with these amines can be done at 60 °C to cut the displacement time to 2 h and the acylation time to 2 min each. With these optimized methods, the solid-phase coupling efficiency for quaternary-ammonium-type peptoid monomers exceeds 95%, as demonstrated in the crude HPLC traces of peptoids **17**−**20** (see Supporting Information for all HPLC traces).

Furthermore, the Net$_2$pgae side-chain can be easily converted on-resin to a triazole with CuAAC "click" chemistry in almost quantitative yield allowing for further diversification of side-chains or postsynthetic conjugation (peptoid **21**). As a proof-of-principle, benzyl azide was conjugated onto Ts-Sar-Net$_2$pgae in high yield (see Supporting Information for further details). This reaction should be compatible with most organo-azide precursors, as the "click" reaction is extraordinarily robust and can facilitate a wide variety of substituents.[61]

We next optimized solid-phase peptoid synthesis with the tertiary-amine-containing side-chains. Unlike the quaternary ammonium side-chains, tertiary-amine side-chains contain nucleophilic tertiary amino groups capable of intramolecular S_N2 with the $i-1$ haloacetyl residue (Scheme 3). Initial attempts at incorporating these side-chains with normal methods resulted in cyclized, ketopiperazinium products. Cyclization yield up to 100% was observed (by HPLC) following bromoacetylation of Net$_2$ae (peptoid **22**), while N^{i}Pr$_2$ae (peptoid **23**) gave ∼40% cyclized product. We minimized the cyclization by acylating with the less electrophilic chloroacetic acid and reducing the reaction time from 30 to 2 min. This strategy reduces the cyclization yield to ∼60% with Net$_2$ae and ∼0% with N^{i}Pr$_2$ae. Although this method still prevents usage of multiple Net$_2$ae residues in longer sequences, the N^{i}Pr$_2$ae residue is now readily incorporated. As a proof of concept, we were able to synthesize pentamer Ts-(N^{i}Pr$_2$ae)$_5$-NH$_2$ (peptoid **24**) in excellent yield (>95%) (see Supporting Information).

Application toward Water-Soluble Ribbon Structures. To demonstrate the utility and potent folding properties of these new monomers, we strived to synthesize long peptoid sequences that are water-soluble, comprise diverse side-chains, and possess defined secondary structures. Such properties are essential for the design of functional peptoid-based materials, such as therapeutics and nanostructures. We were particularly interested in the ribbon structure, previously reported by Blackwell and co-workers, which features alternating *cis* and *trans* backbone−amide bonds. The original ribbon structures (up to 6-mer) were made up of two types of alternating hydrophobic monomers, an Ns1npe side-chain and N-aryl side-chains, which are strong *cis* and *trans* inducers, respectively.[62] This presented an opportunity for us to create an amphiphilic ribbon structure by substituting the bulky and nonpolar *cis* inducers (Ns1npe) with our newly described cationic, water-soluble monomers.[23] Moreover, cationic ammonium moieties have been shown to favorably bind to electron-rich π systems, thus allowing for additional non-covalent interactions that promote folding in our ribbon structures.[63]

We designed two long sequences: a 6-mer peptoid (**25**) where all the Ns1npe are replaced with N^{i}Pr$_2$ae, and a 10-mer, peptoid (**26**), where we installed five of our monomers, Net$_2$pgae, Net$_2$bnae, Net$_3$ae, Nme$_3$ae, and N^{i}Pr$_2$ae, at the Ns1pe positions (Chart 2). Different *N*-aryl monomers were used at the *trans* positions in peptoids **25** and **26** to facilitate peak dispersion in the NMR spectra. Both peptoids were also capped on the N-terminus with formyl, which functions as a well-separated NMR spectroscopic handle (singlet at ∼8 ppm) for determining structural homogeneity.

^{1}H NMR spectroscopy in polar protic solvents (MeOD and D$_2$O) of **25** and **26** reveals only one major conformation (Table 3), as indicated by the distribution of formyl NMR signals. In contrast, a structurally undefined hexamer and decamer would show 2^6 (64) and 2^{10} (1024) amide isomers, respectively. The ^{1}H NMR resonances of **25** and **26** are also well-dispersed, especially in MeOD, indicative of a well-folded structure. ROESY NMR spectroscopy confirms a pattern of alternating *cis*−*trans* amides, consistent the ribbon structure (ω = 0°, 180°, 0°, ...). The high population of the *cis* amides at the cationic residues suggests that CH−O interactions are also operative in the longer peptoid. Moreover, we observed ROESY cross-peaks diagnostic of a ribbon fold between the *i* side-chain and the *i*+3 side-chain (Figure 7a). Note that an alternating *cis*−*trans* amide backbone with a different (ψ, φ) pattern could also produce a "square helix" secondary structure,[24] though this should result in cross-peaks between the *i* and *i*+6 residues,[24] which we do not observe.

DOI: 10.1021/jacs.9b10497
J. Am. Chem. Soc. 2019, 141, 19436−19447

The NMR distance constraints were used for simulated annealing via replica exchange molecular dynamics (REMD) for structural determination of peptoid models corresponding to **26** (Figure 7a). The 10 lowest energy structures are shown in Figure 7b. The stereochemistry of the backbone chain is mostly consistent with that of an extended peptoid ribbon secondary structure, with backbone dihedrals alternating between Z_{Sc} ($\phi = -90°$, $\psi = \pm 180°$, $\omega = 0°$) and Z_{Rt} ($\phi = 90°$, $\psi = \pm 180°$, $\omega = 180°$).[40] Excluding the termini, the mean ϕ and ψ absolute values for the *N*-aryl residues are $|87| \pm 18°$ and $|151| \pm 23°$, respectively, while the mean ϕ and ψ absolute values for the ammonium residues were $|88| \pm 13°$ and $|152| \pm 22°$, respectively. The standard deviations of the ϕ and ψ angles are quite large, indicating that the ensemble, although retaining the stereochemistry of a ribbon, is still highly flexible, perhaps due to the absence of chiral side-chains. Our design hypothesis regarding inter-residual cation → π interactions between *i* and *i*+3 pairs also proved correct. On average, three pairs of cation → π interactions help to stabilize the fold and might explain the higher folded population observed for **26** over **25** in D_2O, as compound **26** can potentially accommodate more cation → π interactions than compound **25**. Moreover, a total of three types of noncovalent interactions (hydrogen bonds, sterics for *N*-aryl residues, and cation → π interactions) work cooperatively to induce folding, and such an ensemble of interactions is reminiscent of protein folding in nature and should actively be used in deriving new biomimetic structures.

SUMMARY AND OUTLOOK

In this report, we demonstrate that this new class of monomers, i.e., cationic alkyl ammonium ethyl side chains, have the unique ability to control rotation about ω to an extraordinary degree while being diverse, hydrophilic, and amenable to solid-phase synthesis, unlike previously reported steric and electronic methods to *cis* induction. These peptoid side-chains leverage an unusual mechanism to enforce the *cis*-amide conformation via an ensemble of several weak CH−O bonds between the side-chains and the backbone carbonyls. This method is in contrast to the traditional approach of controlling peptoid *cis*/*trans* isomerization, by tuning a single interaction between the side-chain and the backbone. The present contribution suggests that a shift in design strategy toward multiple, cooperative forces may be beneficial in paving the road toward generating new, diverse monomers that promote predictable peptoid architectures.

Given the biological relevance of peptoids, structural integrity and solubility in water are crucial for application development. These peptoid submonomers are readily available and easily diversifiable via simple synthesis and amenable to solid-phase peptoid synthesis, which allows for their incorporation into peptoid libraries and longer chains of sequence-defined polymers. We also reported optimized synthesis conditions to incorporate these monomers into a peptoid sequence in over 95% yield along with "click" methodology to convert Net_2pgae into its triazole form. We further demonstrate application of these new monomers to create the longest known example of Blackwell's ribbon peptoid secondary structure.[23] Re-engineering of other structures from literature, such as the PPI helix,[19−21] peptoid square helix,[24] and nanosheets, along with the development of chiral versions of these monomers are currently underway.

ASSOCIATED CONTENT

Supporting Information

The Supporting Information is available free of charge at https://pubs.acs.org/doi/10.1021/jacs.9b10497.

Full synthetic, physical, theoretical, and crystallographic details (PDF)

X-ray crystallographic data for **8**·BPh_4 (CIF)

X-ray crystallographic data for **11**·BPh_4 (CIF)

X-ray crystallographic data for **16**·BPh_4 (CIF)

NMR structure of **26** (PDB)

AUTHOR INFORMATION

Corresponding Authors

*ainguyen@lbl.gov

*rnzuckermann@lbl.gov

ORCID

Andy I. Nguyen: 0000-0003-4137-6453

Ryan K. Spencer: 0000-0002-1043-3913

Ronald N. Zuckermann: 0000-0002-3055-8860

Author Contributions

⊥A.W.W. and A.I.N. contributed equally.

Notes

The authors declare no competing financial interest.

ACKNOWLEDGMENTS

Work at the Molecular Foundry was supported by the Office of Science, Office of Basic Energy Sciences, of the U.S. Department of Energy under Contract No. DE-AC02-05CH11231. Additional support was provided by the DARPA Fold F(x) program. DFT calculations were carried out on the High Performance Computing resources at New York University Abu Dhabi. The funds for the 900 MHz NMR spectrometer in the QB3 Institute at University of California, Berkeley, were provided by the NIH Grant GM68933. Additionally, we would like to thank Dr. Nicholas Settineri of the UC Berkeley CheXray facility for his assistance in X-ray diffraction studies, Dr. Jeff G. Pelton for his assistance in NMR studies, and Victor R. Mann, Michael Connolly, and Zeming Wang for helpful discussions.

REFERENCES

(1) Zuckermann, R. N.; Kerr, J. M.; Kent, S. B. H.; Moos, W. H. Efficient method for the preparation of peptoids [oligo(N-substituted glycines)] by submonomer solid-phase synthesis. *J. Am. Chem. Soc.* **1992**, *114*, 10646−10647.

(2) Yoo, B.; Kirshenbaum, K. Peptoid architectures: elaboration, actuation, and application. *Curr. Opin. Chem. Biol.* **2008**, *12*, 714−721.

(3) Fowler, S. A.; Blackwell, H. E. Structure−function relationships in peptoids: Recent advances toward deciphering the structural requirements for biological function. *Org. Biomol. Chem.* **2009**, *7*, 1508−1524.

(4) Miller, S. M. S.; Reyna, J.; Ng, S.; Zuckermann, R. N.; Kerr, J. M.; Moos, W. H. Proteolytic studies of homologous peptide and N-substituted glycine peptoid oligomers. *Bioorg. Med. Chem. Lett.* **1994**, *4*, 2657−262.

(5) Vollrath, S. B. L.; Fürniss, D.; Schepers, U.; Bräse, S. Amphiphilic peptoid transporters − synthesis and evaluation. *Org. Biomol. Chem.* **2013**, *11*, 8197−8201.

(6) Kwon, Y.-U.; Kodadek, T. Quantitative Evaluation of the Relative Cell Permeability of Peptoids and Peptides. *J. Am. Chem. Soc.* **2007**, *129*, 1508−1509.

DOI: 10.1021/jacs.9b10497
J. Am. Chem. Soc. 2019, 141, 19436−19447

(7) Huang, M. L.; Ehre, D.; Jiang, Q.; Hu, C.; Kirshenbaum, K.; Ward, M. D. Biomimetic peptoid oligomers as dual-action antifreeze agents. *Proc. Natl. Acad. Sci. U. S. A.* **2012**, *109*, 19922.
(8) Zuckermann, R.; Kodadek, T. Peptoids as Potential Therapeutics. *Curr. Op. Mol. Ther.* **2009**, *11*, 299−307.
(9) Mojsoska, B.; Carretero, G.; Larsen, S.; Mateiu, R. V.; Jenssen, H. Peptoids successfully inhibit the growth of gram negative E. coli causing substantial membrane damage. *Sci. Rep.* **2017**, *7*, 42332.
(10) Chongsiriwatana, N. P.; Patch, J. A.; Czyzewski, A. M.; Dohm, M. T.; Ivankin, A.; Gidalevitz, D.; Zuckermann, R. N.; Barron, A. E. Peptoids that mimic the structure, function, and mechanism of helical antimicrobial peptides. *Proc. Natl. Acad. Sci. U. S. A.* **2008**, *105*, 2794−2799.
(11) Jun, J. M. V.; Altoe, M. V. P.; Aloni, S.; Zuckermann, R. N. Peptoid nanosheets as soluble, two-dimensional templates for calcium carbonate mineralization. *Chem. Commun.* **2015**, *51*, 10218−10221.
(12) Mannige, R. V.; Haxton, T. K.; Proulx, C.; Robertson, E. J.; Battigelli, A.; Butterfoss, G. L.; Zuckermann, R. N.; Whitelam, S. Peptoid nanosheets exhibit a new secondary-structure motif. *Nature* **2015**, *526*, 415.
(13) Mu, P.; Zhou, G.; Chen, C.-L. 2D nanomaterials assembled from sequence-defined molecules. *Nano-Struct. Nano-Obj.* **2018**, *15*, 153−166.
(14) Sun, J.; Jiang, X.; Lund, R.; Downing, K. H.; Balsara, N. P.; Zuckermann, R. N. Self-assembly of crystalline nanotubes from monodisperse amphiphilic diblock copolypeptoid tiles. *Proc. Natl. Acad. Sci. U. S. A.* **2016**, *113*, 3954−3959.
(15) Vollrath, S. B. L.; Hu, C.; Bräse, S.; Kirshenbaum, K. Peptoid nanotubes: an oligomer macrocycle that reversibly sequesters water via single-crystal-to-single-crystal transformations. *Chem. Commun.* **2013**, *49*, 2317−2319.
(16) Yan, F.; Liu, L.; Walsh, T. R.; Gong, Y.; El-Khoury, P. Z.; Zhang, Y.; Zhu, Z.; De Yoreo, J. J.; Engelhard, M. H.; Zhang, X.; Chen, C.-L. Controlled synthesis of highly-branched plasmonic gold nanoparticles through peptoid engineering. *Nat. Commun.* **2018**, *9*, 2327.
(17) Battigelli, A.; Kim, J. H.; Dehigaspitiya, D. C.; Proulx, C.; Robertson, E. J.; Murray, D. J.; Rad, B.; Kirshenbaum, K.; Zuckermann, R. N. Glycosylated Peptoid Nanosheets as a Multivalent Scaffold for Protein Recognition. *ACS Nano* **2018**, *12*, 2455−2465.
(18) Jin, H.; Ding, Y.-H.; Wang, M.; Song, Y.; Liao, Z.; Newcomb, C. J.; Wu, X.; Tang, X.-Q.; Li, Z.; Lin, Y.; Yan, F.; Jian, T.; Mu, P.; Chen, C.-L. Designable and dynamic single-walled stiff nanotubes assembled from sequence-defined peptoids. *Nat. Commun.* **2018**, *9*, 270.
(19) Armand, P.; Kirshenbaum, K.; Falicov, A.; Dunbrack, R. L.; Dill, K. A.; Zuckermann, R. N.; Cohen, F. E. Chiral N-substituted glycines can form stable helical conformations. *Folding Des.* **1997**, *2*, 369−375.
(20) Stringer, J. R.; Crapster, J. A.; Guzei, I. A.; Blackwell, H. E. Extraordinarily Robust Polyproline Type I Peptoid Helices Generated via the Incorporation of α-Chiral Aromatic *N*-1-Naphthylethyl Side Chains. *J. Am. Chem. Soc.* **2011**, *133*, 15559−15567.
(21) Roy, O.; Dumonteil, G.; Faure, S.; Jouffret, L.; Kriznik, A.; Taillefumier, C. Homogeneous and Robust Polyproline Type I Helices from Peptoids with Nonaromatic α-Chiral Side Chains. *J. Am. Chem. Soc.* **2017**, *139*, 13533−13540.
(22) Wu, C. W.; Kirshenbaum, K.; Sanborn, T. J.; Patch, J. A.; Huang, K.; Dill, K. A.; Zuckermann, R. N.; Barron, A. E. Structural and Spectroscopic Studies of Peptoid Oligomers with α-Chiral Aliphatic Side Chains. *J. Am. Chem. Soc.* **2003**, *125*, 13525−13530.
(23) Crapster, J. A.; Guzei, I. A.; Blackwell, H. E. A Peptoid Ribbon Secondary Structure. *Angew. Chem., Int. Ed.* **2013**, *52*, 5079−5084.
(24) Gorske, B. C.; Mumford, E. M.; Gerrity, C. G.; Ko, I.; Peptoid Square, A. Helix via Synergistic Control of Backbone Dihedral Angles. *J. Am. Chem. Soc.* **2017**, *139*, 8070−8073.
(25) Gorske, B. C.; Stringer, J. R.; Bastian, B. L.; Fowler, S. A.; Blackwell, H. E. New Strategies for the Design of Folded Peptoids Revealed by a Survey of Noncovalent Interactions in Model Systems. *J. Am. Chem. Soc.* **2009**, *131*, 16555−16567.
(26) Roy, O.; Caumes, C.; Esvan, Y.; Didierjean, C.; Faure, S.; Taillefumier, C. The tert-Butyl Side Chain: A Powerful Means to Lock Peptoid Amide Bonds in the Cis Conformation. *Org. Lett.* **2013**, *15*, 2246−2249.
(27) Caumes, C.; Roy, O.; Faure, S.; Taillefumier, C. The Click Triazolium Peptoid Side Chain: A Strong cis-Amide Inducer Enabling Chemical Diversity. *J. Am. Chem. Soc.* **2012**, *134*, 9553−9556.
(28) Shyam, R.; Nauton, L.; Angelici, G.; Roy, O.; Taillefumier, C.; Faure, S. NCα-gem-dimethylated peptoid side chains: A novel approach for structural control and peptide sequence mimetics. *Biopolymers* **2019**, *110*, e23273.
(29) Gimenez, D.; Zhou, G.; Hurley, M. F. D.; Aguilar, J. A.; Voelz, V. A.; Cobb, S. L. Fluorinated Aromatic Monomers as Building Blocks To Control α-Peptoid Conformation and Structure. *J. Am. Chem. Soc.* **2019**, *141*, 3430−3434.
(30) Gimenez, D.; Aguilar, J. A.; Bromley, E. H. C.; Cobb, S. L. Stabilising Peptoid Helices Using Non-Chiral Fluoroalkyl Monomers. *Angew. Chem., Int. Ed.* **2018**, *57*, 10549−10553.
(31) Laursen, J. S.; Engel-Andreasen, J.; Fristrup, P.; Harris, P.; Olsen, C. A. Cis−Trans Amide Bond Rotamers in β-Peptoids and Peptoids: Evaluation of Stereoelectronic Effects in Backbone and Side Chains. *J. Am. Chem. Soc.* **2013**, *135*, 2835−2844.
(32) Laurence, C.; Berthelot, M. Observations on the strength of hydrogen bonding. *Perspect. Drug Discovery Des.* **2000**, *18*, 39−60.
(33) Petukhov, M.; Rychkov, G.; Firsov, L.; Serrano, L. H-bonding in protein hydration revisited. *Protein Sci.* **2004**, *13*, 2120−2129.
(34) Roe, L. T.; Pelton, J. G.; Edison, J. R.; Butterfoss, G. L.; Tresca, B. W.; LaFaye, B. A.; Whitelam, S.; Wemmer, D. E.; Zuckermann, R. N. Unconstrained peptoid tetramer exhibits a predominant conformation in aqueous solution. *Biopolymers* **2019**, *0*, e23267.
(35) Nguyen, A. I.; Spencer, R. K.; Anderson; Christopher, L.; Zuckermann, R. N. A bio-inspired approach to ligand design: folding single-chain peptoids to chelate a multimetallic cluster. *Chem. Sci.* **2018**, *9*, 8806−8813.
(36) Fuller, A. A.; Yurash, B. A.; Schaumann, E. N.; Seidl, F. J. Self-Association of Water-Soluble Peptoids Comprising (*S*)-*N*-1-(Naphthylethyl)glycine Residues. *Org. Lett.* **2013**, *15*, 5118−5121.
(37) Frisch, M. J.; Trucks, G. W.; Schlegel, H. B.; Scuseria, G. E.; Robb, M. A.; Cheeseman, J. R.; Scalmani, G.; Barone, V.; Petersson, G. A.; Nakatsuji, H.; Li, X.; Caricato, M.; Marenich, A. V.; Bloino, J.; Janesko, B. G.; Gomperts, R.; Mennucci, B.; Hratchian, H. P.; V, J.; Ortiz, A. F. I.; Sonnenberg, J. L.; Williams-Young, D.; Ding, F.; Lipparini, F.; Egidi, F.; Goings, J.; Peng, B.; Petrone, A.; Henderson, T.; Ranasinghe, D.; Zakrzewski, V. G.; Gao, J.; Rega, N.; Zheng, G.; Liang, W.; Hada, M.; Ehara, M.; Toyota, K.; Fukuda, R.; Hasegawa, J.; Ishida, M.; Nakajima, T.; Honda, Y.; Kitao, O.; Nakai, H.; Vreven, T.; Throssell, K.; Montgomery, J. A., Jr.; Peralta, J. E.; Ogliaro, F.; Bearpark, M. J.; Heyd, J. J.; Brothers, E. N.; Kudin, K. N.; Staroverov, V. N.; Keith, T. A.; Kobayashi, R.; Normand, J.; Raghavachari, K.; Rendell, A. P.; Burant, J. C.; Iyengar, S. S.; Tomasi, J.; Cossi, M.; Millam, J. M.; Klene, M.; Adamo, C.; Cammi, R.; Ochterski, J. W.; Martin, R. L.; Morokuma, K.; Farkas, O.; Foresman, J. B.; Fox, D. J. *Gaussian 16, Revision B.01*; Gaussian, Inc.: Wallingford, CT, 2016.
(38) Shirakawa, S.; Liu, S.; Kaneko, S.; Kumatabara, Y.; Fukuda, A.; Omagari, Y.; Maruoka, K. Tetraalkylammonium Salts as Hydrogen-Bonding Catalysts. *Angew. Chem., Int. Ed.* **2015**, *54*, 15767−15770.
(39) Holub, J. M.; Kirshenbaum, K. Tricks with clicks: modification of peptidomimetic oligomers via copper-catalyzed azide-alkyne [3 + 2] cycloaddition. *Chem. Soc. Rev.* **2010**, *39*, 1325−1337.
(40) Spencer, R. K.; Butterfoss, G. L.; Edison, J. R.; Eastwood, J. R.; Whitelam, S.; Kirshenbaum, K.; Zuckermann, R. N. Stereochemistry of polypeptoid chain configurations. *Biopolymers* **2019**, *110*, e23266.
(41) Park, S. H.; Szleifer, I. Structural and Dynamical Characteristics of Peptoid Oligomers with Achiral Aliphatic Side Chains Studied by Molecular Dynamics Simulation. *J. Phys. Chem. B* **2011**, *115*, 10967−10975.

DOI: 10.1021/jacs.9b10497
J. Am. Chem. Soc. 2019, 141, 19436−19447

(42) Wahl, M. C.; Sundaralingam, M. C-H···O hydrogen bonding in biology. *Trends Biochem. Sci.* **1997**, *22*, 97−102.
(43) Yokoyama, T.; Mizuguchi, M.; Nabeshima, Y.; Kusaka, K.; Yamada, T.; Hosoya, T.; Ohhara, T.; Kurihara, K.; Tomoyori, K.; Tanaka, I.; Niimura, N. Hydrogen-bond network and pH sensitivity in transthyretin: Neutron crystal structure of human transthyretin. *J. Struct. Biol.* **2012**, *177*, 283−290.
(44) Ramachandran, G. X.; Chandrasekharan, R. Interchain hydrogen bonds via bound water molecules in the collagen triple helix. *Biopolymers* **1968**, *6*, 1649−1658.
(45) Scheiner, S.; Kar, T.; Gu, Y. Strength of the Cα H··O Hydrogen Bond of Amino Acid Residues. *J. Biol. Chem.* **2001**, *276*, 9832−9837.
(46) Steiner, G. D. a. T. *The Weak Hydrogen Bond In Structural Chemistry and Biology*; Oxford University Press: Oxford, 2001.
(47) Laliberté, D.; Maris, T.; Wuest, J. D. Molecular networks built from weakly interacting nitro-substituted pentaerythrityl tetraaryl ethers. *CrystEngComm* **2005**, *7*, 158−160.
(48) Iwase, S.; Xiang, B.; Ghosh, S.; Ren, T.; Lewis, P. W.; Cochrane, J. C.; Allis, C. D.; Picketts, D. J.; Patel, D. J.; Li, H.; Shi, Y. ATRX ADD domain links an atypical histone methylation recognition mechanism to human mental-retardation syndrome. *Nat. Struct. Mol. Biol.* **2011**, *18*, 769.
(49) Stamos, J.; Sliwkowski, M. X.; Eigenbrot, C. Structure of the Epidermal Growth Factor Receptor Kinase Domain Alone and in Complex with a 4-Anilinoquinazoline Inhibitor. *J. Biol. Chem.* **2002**, *277*, 46265−46272.
(50) Horowitz, S.; Trievel, R. C. Carbon-Oxygen Hydrogen Bonding in Biological Structure and Function. *J. Biol. Chem.* **2012**, *287*, 41576−41582.
(51) Jeffrey, G. A. *An Introduction to Hydrogen Bonding*; Oxford University Press: New York, 1997.
(52) Pimentel, G. C.; McClellan, A. L. *The Hydrogen Bond*; W.H. Freeman, 1960.
(53) Cannizzaro, C. E.; Houk, K. N. Magnitudes and Chemical Consequences of R3N+−C−H···OC Hydrogen Bonding. *J. Am. Chem. Soc.* **2002**, *124*, 7163−7169.
(54) Pike, S. J.; Lavagnini, E.; Varley, L. M.; Cook, J. L.; Hunter, C. A. H-Bond donor parameters for cations. *Chem. Sci.* **2019**, *10*, 5943−5951.
(55) Arbely, E.; Arkin, I. T. Experimental Measurement of the Strength of a Cα−H···O Bond in a Lipid Bilayer. *J. Am. Chem. Soc.* **2004**, *126*, 5362−5363.
(56) Musah, R. A.; Jensen, G. M.; Rosenfeld, R. J.; McRee, D. E.; Goodin, D. B.; Bunte, S. W. Variation in Strength of an Unconventional C−H to O Hydrogen Bond in an Engineered Protein Cavity. *J. Am. Chem. Soc.* **1997**, *119*, 9083−9084.
(57) Silverstein, T. P. The Real Reason Why Oil and Water Don't Mix. *J. Chem. Educ.* **1998**, *75*, 116.
(58) Frausto da Silva, J. J. R. The chelate effect redefined. *J. Chem. Educ.* **1983**, *60*, 390.
(59) Vallet, V.; Wahlgren, U.; Grenthe, I. Chelate Effect and Thermodynamics of Metal Complex Formation in Solution: A Quantum Chemical Study. *J. Am. Chem. Soc.* **2003**, *125*, 14941−14950.
(60) Good, N. E.; Winget, G. D.; Winter, W.; Connolly, T. N.; Izawa, S.; Singh, R. M. M. Hydrogen Ion Buffers for Biological Research*. *Biochemistry* **1966**, *5*, 467−477.
(61) Meldal, M.; Tornøe, C. W. Cu-Catalyzed Azide−Alkyne Cycloaddition. *Chem. Rev.* **2008**, *108*, 2952−3015.
(62) Shah, N. H.; Butterfoss, G. L.; Nguyen, K.; Yoo, B.; Bonneau, R.; Rabenstein, D. L.; Kirshenbaum, K. Oligo(*N*-aryl glycines): A New Twist on Structured Peptoids. *J. Am. Chem. Soc.* **2008**, *130*, 16622−16632.
(63) Dougherty, D. A. The cation-π interaction. *Acc. Chem. Res.* **2013**, *46*, 885−893.

DOI: 10.1021/jacs.9b10497
J. Am. Chem. Soc. 2019, 141, 19436−19447